



Multiscale multifractal DCCA and complexity behaviors of return intervals for Potts price model

Jie Wang^{a,b,*}, Jun Wang^a, H. Eugene Stanley^b

^a Institute of Financial Mathematics and Financial Engineering, School of Science, Beijing Jiaotong University, Beijing 100044, PR China

^b Center for Polymer Studies and Department of Physics, Boston University, Boston, MA 02215, USA

HIGHLIGHTS

- A Potts financial model is developed to investigate volatility of return intervals.
- MM-DCCA based on Hurst surface is developed to analyze cross-correlation of return intervals.
- Using Lempel–Ziv complexity to illustrate complexity of return intervals in different scales.
- Empirical research shows the feasibility of proposed model in cross-correlation and complexity.

ARTICLE INFO

Article history:

Received 11 August 2017

Received in revised form 9 October 2017

Available online 16 November 2017

Keywords:

Return intervals

Potts price model

Multiscale multifractal DCCA

Lempel–Ziv complexity

Statistical physics

ABSTRACT

To investigate the characteristics of extreme events in financial markets and the corresponding return intervals among these events, we use a Potts dynamic system to construct a random financial time series model of the attitudes of market traders. We use multiscale multifractal detrended cross-correlation analysis (MM-DCCA) and Lempel–Ziv complexity (LZC) perform numerical research of the return intervals for two significant China's stock market indices and for the proposed model. The new MM-DCCA method is based on the Hurst surface and provides more interpretable cross-correlations of the dynamic mechanism between different return interval series. We scale the LZC method with different exponents to illustrate the complexity of return intervals in different scales. Empirical studies indicate that the proposed return intervals from the Potts system and the real stock market indices hold similar statistical properties.

© 2017 Elsevier B.V. All rights reserved.

1. Introduction

The financial market is a complex and highly volatile evolving dynamic system, and its corresponding financial time series are inherently noisy, non-stationary, and chaotic. The statistical properties of price fluctuations [1–7] are essential when analyzing and modeling financial market dynamics, which has long been a focus of economic research. Stock volatility is of interest to traders because it quantifies risk, optimizes portfolios [8–13], and is a key input in such option pricing models as the Black–Scholes [14]. Understanding that the primary causes of price movements are the arrival of new information and interactions among market investors, a number of different market models have been introduced in an attempt to reproduce and analyze the fluctuation behavior of stock markets [15–19]. A variety of financial price dynamics models have been successfully used in modeling the financial markets based on the field of statistical physics systems or interacting

* Corresponding author at: Institute of Financial Mathematics and Financial Engineering, School of Science, Beijing Jiaotong University, Beijing 100044, PR China.

E-mail addresses: wangjie@bjtu.edu.cn, jiewang@bu.edu (J. Wang).

particle systems, to model the main observed features of price dynamics, or the so called stylized facts, such as fat-tailed distribution of returns, volatility clustering and multifractality [9–12,14,17]. Stauffer and Penna [20] and Yu and Wang [21] have developed price models using lattice percolation and lattice-oriented percolation in which a percolation cluster defines a group of traders who share the same market trading attitude. Zhang and Wang [22] used the stochastic contact system to develop a random financial stock price model in which the epidemic spreading of the contact model defines the spread of a stock market investment attitude among traders. Empirical results indicate that these simulative models reflect the statistical characteristics of actual stock markets.

Here we employ the Potts model to simulate and characterize the time evolution of a market time series. This is a famous statistical physics approach to modeling nonequilibrium statistical mechanics and is an extension of the Ising model [23–26]. We use a two-dimensional 3-state Potts model to develop a stock price time series model. Like the Ising model, the Potts model has a second-order phase transition that separates a low-temperature ordered phase from a high-temperature disordered phase. In this proposed financial model, the subunits in a two-dimensional Potts model are designated spins or agents (with interactions between nearest neighbors), and the clusters of parallel spins in the square-lattice Potts model are designated groups of market traders acting together.

Wang et al. [27] examined high-frequency financial data, studied the return intervals between price volatilities, and found that the probability density function of return intervals follows a scaling function. Here we use the Lempel–Ziv complexity (LZC) to explore the complex, dynamic behavior of the return intervals in the proposed Potts financial model and in real stock markets. The LZC [28–30] is a non-parametric measure of complexity in a one-dimensional signal that is related to the number of distinct substrings and the rate of their recurrence. Some empirical studies have investigated the non-parametric measure of complexity in a one-dimensional signal that is related to the number of distinct substrings and the rate of their recurrence. Empirical studies have investigated the scaling behavior of financial data [31,32], and several models have been proposed to account for the observed multifractal features [33–35]. Zhou [36] extended multifractal detrended fluctuation analysis (MF-DFA) to two time series in order to obtain the multifractal features in the powerlaw cross-correlations between them, and they designated it multifractal detrended cross-correlation analysis (MF-DCCA). Zebende [37] proposed a coefficient with the objective of quantifying the level of cross-correlation between nonstationary time series. da Silva et al. [38] applied the detrended cross-correlation coefficient at the Brazil stock market. We here develop and use method multiscale MF-DCCA (MM-DCCA) to investigate the multifractal behaviors of cross-correlations between two return interval series. The goal is to apply LZC and MM-DCCA methods and investigate the complexity, multifractality, and cross-correlation properties of the return interval time series of simulation data and of real stock markets.

2. Financial time series model

2.1. Brief description of Potts model

The Potts model is one of the statistical physics systems [39–41] proposed by Potts in the early 1950s. An extension of the Ising model to more than two components, the model with general Q components bears its current name. The Potts model is related to a number of outstanding problems in lattice statistics, and its critical behavior is richer and more general than that of the Ising model. We consider the two-dimensional integer lattice \mathbb{Z}^2 and denote by \mathfrak{B} the set of bonds of the lattice (pairs of nearest neighbors). In the Q -state Potts model, we let $\Omega_{\mathbb{Z}^2} = \{1, 2, \dots, Q\}^{\mathbb{Z}^2}$ denote the space of spin configurations on \mathbb{Z}^2 , an element of $\Omega_{\mathbb{Z}^2}$ usually notated $\sigma = \{\sigma_i : i \in \mathbb{Z}^2\}$. The spin σ_i take on one-integer values from 1 to Q , and the Q is a parameter of the model. For every $\sigma \in \Omega_{\mathbb{Z}^2}$, the Hamiltonian system of the Q -state Potts model ($J > 0$) is

$$H_{\mathbb{Z}^2,b}(\sigma) = -J \sum_{(i,j)} \delta_{\sigma_i,\sigma_j} - b \sum_i \delta_{\sigma_i,1}, \quad (1)$$

where δ is the Kronecker symbol, $\delta_{\sigma_i,\sigma_j} = 1$ only when $\sigma_i = \sigma_j$, (i, j) denotes pairs of nearest-neighbor spins on the lattice, and the applied magnetic field b acts on the (arbitrarily chosen) state 1. Then the partition function is

$$Z_{\mathbb{Z}^2,h}(\sigma) = \sum \exp\left(K \sum_{(i,j)} \delta_{\sigma_i,\sigma_j} + h \sum_i \delta_{\sigma_i,1}\right), \quad (2)$$

where $K = \beta J$ and $h = \beta b$, $\beta = 1/(k_B T)$, and k_B and T are the Boltzmann constant and temperature, respectively. In what follows we consider the Q -state Potts model with no external magnetic field ($b = 0$ and $h = 0$). When $d \geq 2$ the model sustains an order–disorder transition, and the critical value is $\beta_c = \ln(1 + \sqrt{Q})$ in $d = 2$. When $\beta > \beta_c$ the Q -fold permutation symmetry of Eq. (1) is broken, and one of the Q different ground states is singled out. When $Q = 2$ the model is the familiar Ising model with a second-order transition.

2.2. Financial price time series model

We here use a two-dimensional 3-state Potts model on a $L \times L$ lattice to produce a financial agent-based price model. Here the strength of interactions between neighboring elements is extremely important. It varies according to their location in the lattice and, as typical of Potts models, small changes in interaction rules do not change the cooperative properties.

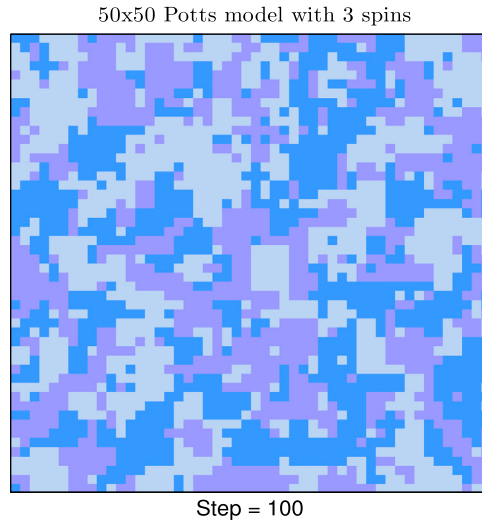


Fig. 1. Graphical illustration of Potts model with $\beta \approx \beta_c$.

Although the optimal number of states allowed in the proposed model is thus not restricted to 3, we use a 3-state Potts financial model that imitates (i) traders taking a selling position, (ii) traders taking a buying position, and (iii) traders taking no trading position, which we classify as type 1, type 2, and type 3, respectively. We assume that stock price behavior is strongly affected by the number of traders $\omega^{(1)}(t)$ (traders of type 1), $\omega^{(2)}(t)$ (traders of type 2), and $\omega^{(3)}(t)$ (traders of type 3). We consider a single stock and assume that there are L^2 traders of this stock who are located in a square-lattice $L \times L \subset \mathbb{Z}^2$, and that each trader can trade a unit number of stock at each time $t \in \{1, 2, \dots, T\}$. At each time t , the fluctuation of stock price process is strongly influenced by the number of traders who take buying positions and the number of traders who take selling positions. When the number of traders in selling positions is smaller than the number of traders in buying positions, the stock price is considered low by market participants, and the stock price gradually increases. The similar is true in the opposite case. Let ω_{ij} be the investing position of a trader ($1 \leq i \leq L, 1 \leq j \leq L$) at time t , and $\omega(t) = (\omega_{11}(t), \dots, \omega_{1L}(t), \dots, \omega_{L1}(t), \dots, \omega_{LL}(t))$ be the configuration of positions for L^2 traders. A space of all configurations of positions for L^2 traders from time 1 to t is given by $\mathcal{W} = \{\omega : \omega = (\omega(1), \dots, \omega(t))\}$. For a given configuration $\omega \in \mathcal{W}$ and a trading day t , let $M^{(k)}(\omega(t)) = |\omega^{(k)}(t)|$ ($k = 1, 2, 3$), which represents the number of $\omega^{(1)}(t)$, $\omega^{(2)}(t)$, and $\omega^{(3)}(t)$ at time t , respectively. Here we assume that the price changes are proportional to the difference between demand and supply $M^{(k)}(\omega(t))$ ($k = 1, 2, 3$), which is affected by the intensity parameter β , where β represents the strength of the spread of information. We define a random variable ξ_t with values 1, -1 , 0 when an investor is buying, selling, or neutral with probabilities p_1, p_{-1} or $1 - (p_1 + p_{-1})$, respectively. These investors send a bullish, bearish, or neutral signal into the market. Fig. 1 uses three different colors to show the effect of investors in the proposed Potts financial model with three different attitudes. For clarity we set Step= 100, $L = 50$ and $\beta \approx \beta_c$.

From the above description and [42,43], the stock price at trading day t is defined

$$\mathcal{P}(t) = \exp\left\{\alpha \sum_{k=1}^3 \frac{\mathcal{M}^{(k)}(t)}{L^2}\right\} \mathcal{P}(t-1) \tag{3}$$

$$\mathcal{M}^{(k)}(t) = M^{(k)}(\omega(t)) \times \gamma_k \times \xi_t^k, \tag{4}$$

where $\alpha (> 0)$ is the depth parameter of the market, random variable $\xi_t(x)$ is the agent's trading attitude (buying, selling or neutral) toward the market and γ_k is the effective strength of each attitude of traders in the stock market such that $\gamma_1 + \gamma_2 + \gamma_3 = 1$. $M^{(k)}(\omega(t))$ represents the aggregate demand and supply, divided by L^2 is a process of normalization. Then we have

$$\mathcal{P}(t) = \mathcal{P}(0) \exp\left\{\alpha \sum_{s=1}^t \sum_{k=1}^3 \frac{\mathcal{M}^{(k)}(s)}{L^2}\right\}, \tag{5}$$

where $\mathcal{P}(0)$ is the stock price at time 0. Then the corresponding formula of the stock logarithmic return is

$$r(t) = r_t = \ln \mathcal{P}(t) - \ln \mathcal{P}(t-1), \quad t \in \{1, 2, \dots, T\}. \tag{6}$$

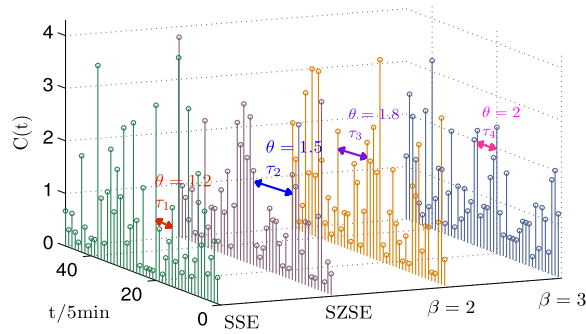


Fig. 2. One-day return interval series of 5-min SSE, SZSE and two simulation series ($\beta = 2, \beta = 3$).

3. Return intervals and data collection

To understand the behavior of financial price fluctuations, the study of scaling properties in financial markets is essential. The behavior of extreme events and the characteristics of return intervals among these events has attracted much recent empirical research [44,45]. In contrast to daily volatility, intraday data exhibit specific patterns caused by differing trading behaviors at different periods during the trading day. Here we do a trend analysis of 5-minute return intervals in the Shanghai Stock Exchange Composite Index (SSE) and the Shenzhen Stock Exchange Component Index (SZSE). We examine the daily closing prices of SSE and SZSE from January 2013 to October 2015. The sampling time is five minutes and the data number size is approximately 32 000.

We let $A(s)$ stand for the intraday pattern, which is the absolute value of price change at a particular moments of the trading day averaged over all N trading days. It is defined

$$A(s) = \sum_{j=1}^L \frac{|r^j(s)|}{N}, \tag{7}$$

where $r^j(s)$ is the logarithmic return at time s of day j . To avoid the impact of the daily fluctuation, the intraday pattern is scaled and becomes

$$\mathcal{R}(t) = \frac{|r(t)|}{A(s)} = \frac{|r^j(s)|}{A(s)}, \tag{8}$$

where $r(t) = r^j(s)$ depends on j and s . The normalized volatility $C(t)$ is defined

$$C(t) = \frac{\mathcal{R}(t)}{\sqrt{E[\mathcal{R}(t)]^2 - (E[\mathcal{R}(t)])^2}}. \tag{9}$$

The threshold θ is measured in units of the standard deviation of $C(t)$.

Fig. 2 shows an example of volatility $C(t)$ with different thresholds θ ($\theta = 1.2, 1.5, 1.8, 2$) for the SSE, the SZSE, and two simulation time series of the model with $\beta = 2$ and $\beta = 3$. We generate a series of five-minute return intervals between those events (denoted by $\{\tau(\theta)\}$). Fig. 2 shows how the return interval time series depends on the threshold θ . We focus on the patterns of return intervals for the different threshold values of $\theta \in \{1.2, 1.5, 1.8, 2\}$. Fig. 3(a) shows the fluctuation of the price time series of the SSE and of two simulation time series with different parameters. Fig. 3(b) shows the return plots $r(t)$ and the corresponding return interval series τ for the SSE and the simulation data.

We next use the Potts financial model and real market data to explore several important fluctuation behaviors in the return interval time series. In our computer simulation we use $L = 100$ with different β parameters, each covering 32 000 data points, in order to compare the simulation data with real-market data of approximately the same size.

4. Complexity of return intervals

4.1. Lempel–Ziv complexity calculation

The Lempel–Ziv complexity (LZC) proposed by Lempel and Ziv [46] is a non-parametric measure of complexity in a one-dimensional signal that is related to the number of distinct substrings and the rate of their recurrence. The LZC is used to evaluate the randomness and complexity of a finite sequences and is closely related to such theoretical properties as entropy and compression ratio. Because LZC analysis uses coarse-grained measurements, the original return interval time series must be transformed into a finite symbol string before calculating the complexity. Here we use the 0-1-2 sequence

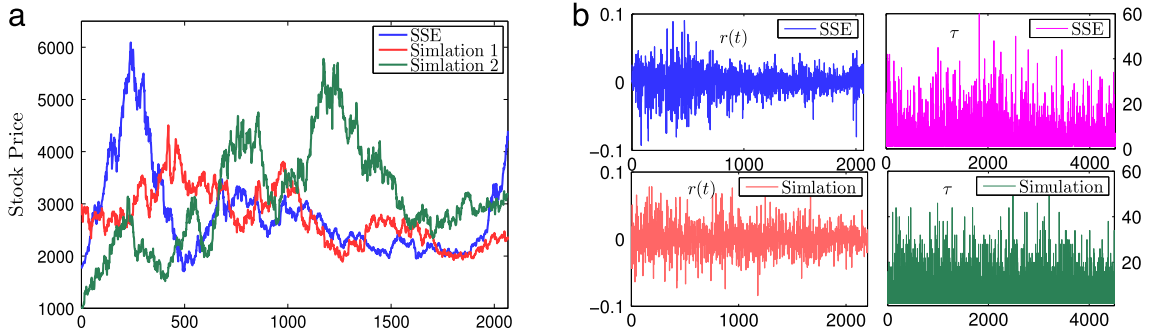


Fig. 3. (a) Price time series of SSE and the simulation price time series of the model. (b) Plots of return series $r(t)$ and the corresponding return interval series τ for SSE and the simulation data of the model.

conversion in order to retain more original data information during the coarse-graining process. We calculate the median x_m , maximum x_{max} , and minimum x_{min} for each of return interval time series and obtain two thresholds: $T_{d_1} = x_m - |x_{min}|/16$ and $T_{d_2} = x_m + |x_{max}|/16$. We compare them with threshold T_{d_1}, T_{d_2} and convert the original time series samples into a 0-1-2 sequence $P = \{s(1), s(2), \dots, s(n)\}$, with $s(t)$ defined by [47]

$$s(t) = \begin{cases} 0, & \text{if } x(t) \leq T_{d_1} \\ 1, & \text{if } T_{d_1} < x(t) < T_{d_2} \\ 2, & \text{if } x(t) \geq T_{d_2}. \end{cases} \tag{10}$$

We then scan string P from left to right and increase complexity counter $c(n)$ by one unit each time a new subsequence of consecutive characters is encountered in the scanning process. For a time series $x(t), t \in 1, 2, \dots, n$, we can measure the LZC of $x(t)$ using the following algorithm [28–30]:

- (1) Let S and Q represent two subsequences of the original subsequence P and SQ be a concatenation of S and Q . Here $SQ\pi$ represents the sequence extracted from SQ in which the last character is deleted.
- (2) Let $v(SQ\pi)$ represent the set comprising all the different subsequences of $SQ\pi$.
- (3) At the beginning, set the complexity counter $c(n) = 1, S = s(1), Q = s(2), SQ = \{s(1), s(2)\}$, and $SQ\pi = s(1)$.
- (4) In general we assume that $S = \{s(1), \dots, s(r)\}, Q = s(r + 1)$, so $SQ\pi = \{s(1), \dots, s(r)\}$. If $Q \in v(SQ\pi)$, then Q is a subsequence of $SQ\pi$, not a new sequence.
- (5) S does not change and we renew Q by adding $s(r + 2)$ to Q , i.e., $Q = \{s(r + 1), s(r + 2)\}$, then we determine judge whether Q belongs to $v(SQ\pi)$ or not.
- (6) Repeat steps (4) and (5) until Q no longer belongs to $v(SQ\pi)$ and $Q = \{s(r + 1), \dots, s(r + i)\}$ is no longer a subsequence of $SQ\pi = \{s(1), \dots, s(r + i - 1)\}$ but a new sequence. We thus increase $c(n)$ by one.
- (7) Thereafter S and Q are combined and renewed, becoming $\{s(1), \dots, s(r + i)\}$, and $s(r + i + 1)$, respectively.
- (8) Repeat the previous steps until Q contains the last character, at which time the number of different subsequences is $c(n)$, i.e., is a measure of Lempel–Ziv complexity.

To obtain a complexity measure that is independent of sequence length, we normalize $c(n)$. If the length of the sequence is n and the number of different symbols in the symbol set is γ (here $\gamma = 2$), the upper bound of $c(n)$ is given by $c(n) < n/[(1 - \epsilon_n)\log_\gamma(n)]$ [24], where ϵ_n is a small quantity and $\epsilon_n \rightarrow 0 (n \rightarrow \infty)$. In general, $n/\log_\gamma(n)$ is the upper limit of $c(n)$, where the base of the logarithm is γ , i.e., $\lim_{n \rightarrow \infty} c(n) = b(n) = n/\log_\gamma(n)$, and $c(n)$ can be normalized via $b(n)$, $L(n) = c(n)/b(n)$. Here $L(n)$ is the normalized LZC of $x(t)$ and reflects the increasing rate of new pattern generation along with the sequence and captures the temporal structure of the time series [28,29].

4.2. Empirical research by LZC

We now examine real stock market indices SSE and SZSE and the simulation data of the Potts financial model ($\beta = 2, 3, 4$). We first set $\theta = 1.2, 1.5, 1.8, 2$ and calculate the corresponding return intervals of each index. We next analyze the LZC of the return intervals using different exponents, labeled $(\tau(\theta))^q$. For different values of $q, (\tau(\theta))^q$ are different volatility series that display varying levels of volatility. We calculate the LZC values of $(\tau(\theta))^q$ with q varying from 0.4 to 10. Fig. 4 shows the LZC analysis results of $(\tau(\theta))^q$. Fig. 4(a) shows that when $\theta = 1.2$ and $q = 1$ the LZC values are close to 0.6 for all time series. Increasing q decreases the LZC values, indicating that $(\tau(\theta))^q$ becomes regular and periodic with this increase of q , and that the generation rate of new volatility behaviors also decreases when q increases. The simulation data plots when $\beta = 2, 4$ run throughout the real stock market data, and the plot of $\beta = 3$ is the highest. Fig. 4(b)–(d) indicate that the trend of the LZC plots of the simulation data and of the real data is the same, and that the LZC values of the simulation data are larger than those of SSE and SZSE. Table 1 shows that the LZC values of $(\tau(\theta))^q$ of the real data and the simulation data are close to 0.6 for $q = 0.4, 0.6, 0.8, 1$, which indicate the relatively high rate of new pattern generation in the enlarged return

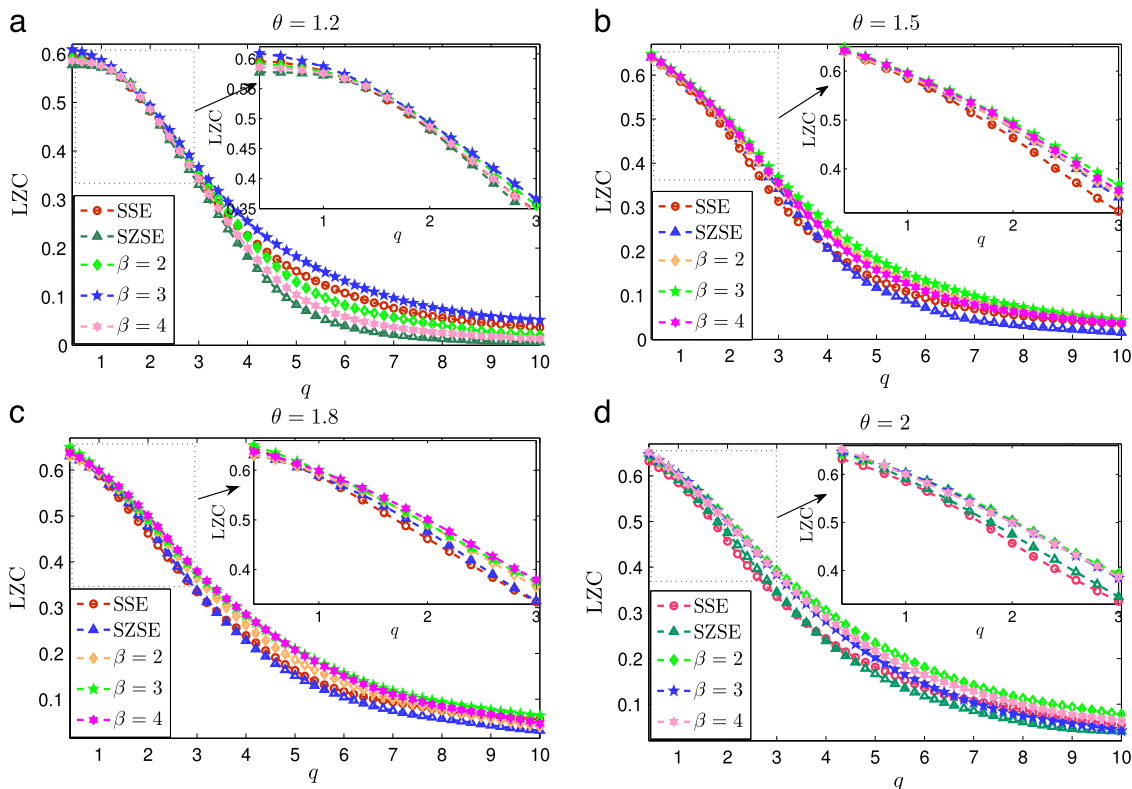


Fig. 4. LZC plots of return intervals with different values of θ from Potts financial model ($\beta = 2, 3, 4$) and the real stock market indexes SSE, SZSE.

Table 1
LZC values of $(\tau(\theta))^q$ with different exponent q .

LZC	SSE	SZSE	$\beta = 2$	$\beta = 3$	$\beta = 4$	SSE	SZSE	$\beta = 2$	$\beta = 3$	$\beta = 4$
$\theta = 1.2$						$\theta = 1.5$				
$q = 0.4$	0.5955	0.5773	0.5920	0.6088	0.5860	0.6401	0.6400	0.6390	0.6472	0.6420
$q = 0.6$	0.5940	0.5760	0.5883	0.6042	0.5839	0.6226	0.6285	0.6241	0.6306	0.6291
$q = 0.8$	0.5878	0.5723	0.5845	0.5962	0.5809	0.6050	0.6088	0.6072	0.6142	0.6120
$q = 1$	0.5798	0.5648	0.5785	0.5867	0.5756	0.5851	0.5915	0.5898	0.5966	0.5953
$q = 2$	0.4821	0.4826	0.4920	0.4928	0.4863	0.4632	0.4817	0.4836	0.4953	0.4899
$q = 3$	0.3446	0.3308	0.3558	0.3662	0.3416	0.3130	0.3422	0.3493	0.3676	0.3561
$q = 4$	0.2261	0.1830	0.2239	0.2550	0.2004	0.2089	0.2064	0.2434	0.2628	0.2387
$q = 5$	0.1526	0.0835	0.1307	0.1825	0.1041	0.1360	0.1176	0.1661	0.1828	0.1574
$q = 6$	0.1075	0.0398	0.0824	0.1322	0.0585	0.0942	0.0723	0.1204	0.1332	0.1099
$\theta = 1.8$						$\theta = 2$				
$q = 0.4$	0.6444	0.6307	0.6305	0.6499	0.6378	0.6321	0.6494	0.6461	0.6467	0.6514
$q = 0.6$	0.6281	0.6217	0.6219	0.6350	0.6278	0.6179	0.6302	0.6302	0.6334	0.6353
$q = 0.8$	0.6082	0.6064	0.6081	0.6179	0.6137	0.6016	0.6113	0.6138	0.6190	0.6182
$q = 1$	0.5874	0.5894	0.5929	0.6003	0.5986	0.5847	0.5910	0.5966	0.6034	0.6004
$q = 2$	0.4619	0.4769	0.4915	0.4920	0.5006	0.4567	0.4752	0.4896	0.5010	0.4998
$q = 3$	0.3342	0.3366	0.3653	0.3748	0.3794	0.3357	0.3452	0.3689	0.3842	0.3862
$q = 4$	0.2387	0.2281	0.2622	0.2827	0.2849	0.2435	0.2387	0.2717	0.2818	0.2904
$q = 5$	0.1628	0.1517	0.1864	0.2098	0.2081	0.1816	0.1668	0.2002	0.2021	0.2173
$q = 6$	0.1166	0.1048	0.1362	0.1563	0.1514	0.1361	0.1180	0.1491	0.1449	0.1645

intervals in both the real data and simulation data. Thus we see the randomness in the increased fluctuation behavior. When $q = 1, 2, 3, 4, 5, 6$, the LZC of $(\tau(\theta))^q$ decreases as q increases, indicating a decrease in randomness in the smaller return intervals. Thus when they are smaller the return intervals become regular and periodic. When $\theta = 1.2$, the maximum LZC value (when $q = 0.4$) is smaller than 0.6 for both real data and simulation data. Inversely, when $\theta = 1.5, 1.8, 2$, the maximum LZC value (when $q = 0.4$) is bigger than 0.6. This indicates that when θ is smaller, the randomness of return interval time series is weaker.

5. Multiscale multifractal detrended cross-correlation

Here we use MM-DCCA to analyze the multifractal features between two cross-correlated non-stationary time series [33,48–50]. This method can simultaneously characterize the monofractality and multifractality of a time series across a wide range of frequencies (scales) and is resistant to nonstationarities. We first describe the MF-DCCA method before introducing the MM-DCCA method.

5.1. Multifractal detrended cross-correlation analysis

We consider two time series $\{x(t)\}$ and $\{y(t)\}$ ($t = 1, 2, \dots, N$), where N is the length of the series. Calculating the profiles of two time series,

$$X_i = \sum_{k=1}^i [x_k - \bar{x}], \quad Y_i = \sum_{k=1}^i [y_k - \bar{y}], \quad i = 1, 2, \dots, N, \tag{11}$$

where \bar{x} and \bar{y} are the averages of two time series $\{x(t)\}$ and $\{y(t)\}$, respectively. We divide $X(i)$ and $Y(i)$ into $N_s = [N/s]$ non-overlapping segments of equal length s . To take the whole series into account, we repeat the same procedure by starting from the opposite end. Thus we get $2N_s$ segments of equal length s and estimate the local trends for each of the $2N_s$ segments using an order m polynomial fit. The corresponding detrended covariance for $v = 1, 2, \dots, N_s$ is

$$F_{DCCA}^2(s, v) = \frac{1}{s} \sum_{j=1}^s |x((v-1)s+j) - x^v(j)| |y((v-1)s+j) - y^v(j)|, \tag{12}$$

and for $v = N_s + 1, N_s + 2, \dots, 2N_s$,

$$F_{DCCA}^2(s, v) = \frac{1}{s} \sum_{j=1}^s |x(N - (v - N_s)s + j) - x^v(j)| |y(N - (v - N_s)s + j) - y^v(j)|. \tag{13}$$

The trends $x^v(j)$ and $y^v(j)$ are the fitting polynomials with order m in segment v . We then average over all segments to obtain the order q fluctuation function

$$F_q(s) = \left\{ \frac{1}{2N_s} \sum_{v=1}^{2N_s} [F_{DCCA}^2(s, v)]^{q/2} \right\}^{1/q}, \quad F_0(s) = \exp\left\{ \frac{1}{4N_s} \ln[F_{DCCA}^2(s, v)] \right\}. \tag{14}$$

To analyze the scaling behavior we study log–log plots of $F_q(s)$ versus s for each value of q . Two cross-correlated series exhibits a power-law expression: $F_q(s) \propto s^{h_{xy}(q)}$. The power-law relationship between the two correlated series is $h_{xy}(q)$. When $h_{xy}(q)$ depends on q there is multifractality, but when the scaling exponent $h_{xy}(q)$ is independent of q the cross-correlations between the two time series are monofractal. In addition, the different scaling of small and large fluctuations makes $h(q)$ strongly dependent on q . When q is positive, segments v with a large variation dominates the average $F_q(s)$. Thus when q is positive, $h(q)$ describes the scaling behavior of the segments with large fluctuations. When q is negative, the segments v with a small variance will dominate the average $F_q(s)$. Thus when $q < 0$ the scaling exponent $h(q)$ describes the scaling behavior of segments with small fluctuations. In particular, when the time series $\{x(t)\}$ is identical to $\{y(t)\}$, the MF-DCCA reverts back to MF-DFA.

5.2. Empirical results by MM-DCCA

Inspired by the work of Gieraltowski et al. [51], we use the Hurst surface method. This is an improved method of analyzing the multifractal cross-correlation between two different non-stationary time series that does not require that we avoid datasets or narrow the range of investigated scales to either only large or only small. Cross-correlations can occur when the analysis is of a data window that is too narrow (finite scale size effect) [52]. They also can occur when there are different correlation features for small and large scales between two different non-stationary time series [53,54]. Both are the case because for extremely low scales $s < 10$ arithmetic underflow often occurs, for scales in the range $s \in [10, 50]$ short-term correlations produce the scaling properties, and for scales $s > 50$ long-term correlations produce the scaling properties.

Here we compare the simulation data of our model with real stock market data. We use a fitting window that moves through the entire range of scales s and obtain a series of overlapped windows. This give us a quasi-continuous change of $h_{xy}(q)$ dependence versus the range of scale s . We place this relationship on a Hurst surface so that the points on the surface represent the generalized dependence $h_{xy}(q, s)$. Note that in the calculation of $h_{xy}(q, s)$ the window itself (the window range) is changed. To present the Hurst surface in a three-dimensional diagram, we calibrate the scale axis using the maximum of the fitting window, which starts at $s = 50$ (i.e., the maximum of the initial scale range [10, 50]) and ends at $s = 600$ (the maximum of the range [120, 600]). We obtain the MF-DCCA results for many fitting windows synchronously, so the dependence $h_{xy}(q, s)$ yields information about the fluctuation levels at different frequency bands, and this allows us to perform a multifractal analysis without any initial time-scale assumptions.

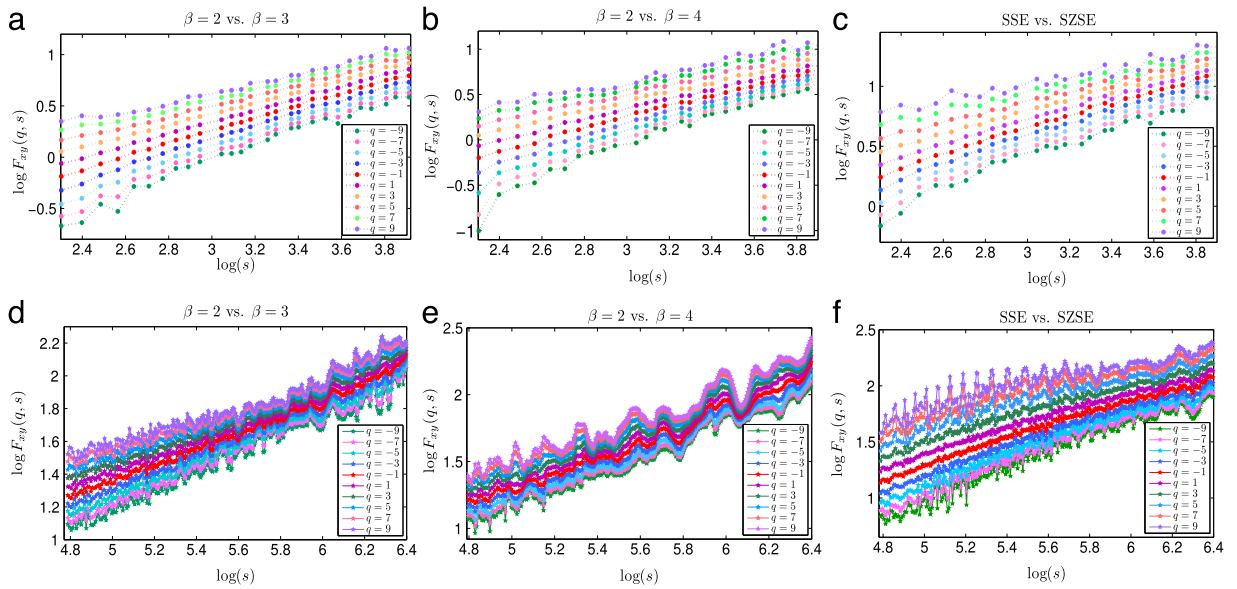


Fig. 5. (a)(b)(c) Fluctuations of $F_q(s)$ versus s with small scale $s \in [10, 50]$ of return intervals for $\theta = 1.2$. (d)(e)(f) Fluctuations of $F_q(s)$ versus s with large scale $s \in [120, 600]$ of return intervals for $\theta = 1.2$.

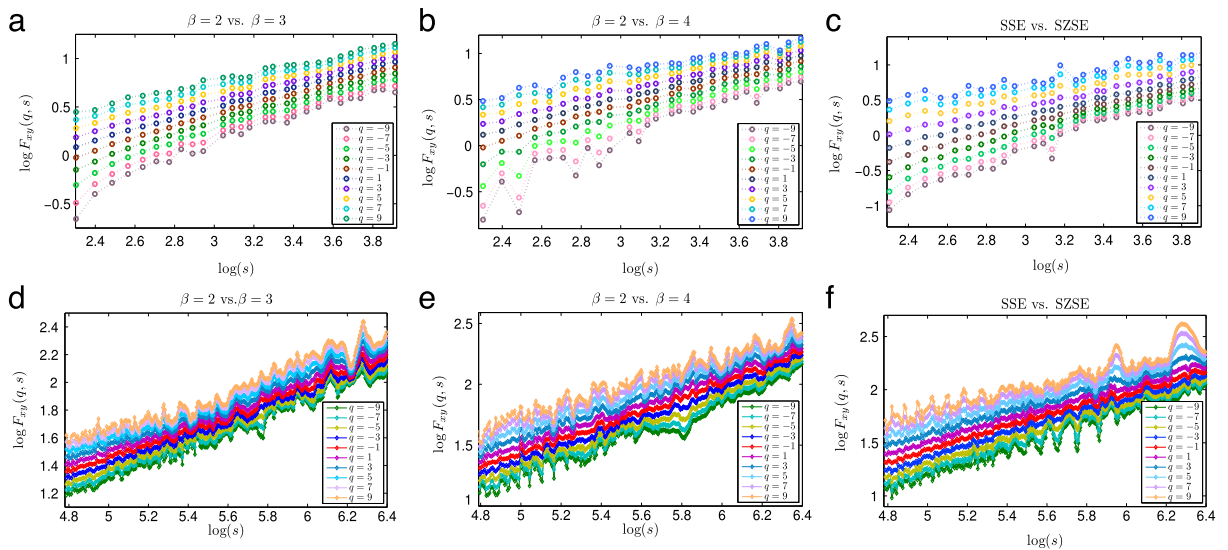


Fig. 6. (a)(b)(c) Fluctuations of $F_q(s)$ versus s with small scale $s \in [10, 50]$ of return intervals for $\theta = 1.5$. (d)(e)(f) Fluctuations of $F_q(s)$ versus s with large scale $s \in [120, 600]$ of return intervals for $\theta = 1.5$.

The empirical data come from the intraday data of {SSE vs. SZSE}, and two pairs of model simulation data with different parameter sets ($\{\beta = 2 \text{ vs. } \beta = 3\}$ and $\{\beta = 3 \text{ vs. } \beta = 4\}$). Because the MM-DCCA method is most effective when the series length is as long as possible, we choose the return interval series $\theta = 1.2$ and $\theta = 1.5$. Examining the log–log plots of $F_q(s)$ in the smallest scale $s \in [10, 50]$ and the largest scale $s \in [120, 600]$, Fig. 5 shows the log–log plots of $F_q(s)$ versus s for the above three pairs of return interval data when $\theta = 1.2$. We analyze the scaling behaviors of fluctuation $F_q(s)$ for different values of q at a small scale $s \in [10, 50]$ and at a large scale $s \in [120, 600]$. Note that the empirical research shows that the correlations of return intervals for different simulation data $\{\beta = 2 \text{ vs. } \beta = 3\}$, $\{\beta = 3 \text{ vs. } \beta = 4\}$ and the real data {SSE vs. SZSE} display cross-correlations similar to power-law scaling and share its fluctuation property. Fig. 6 shows that the cross-correlation fluctuation behaviors are similar in the return interval time series $\{\beta = 2 \text{ vs. } \beta = 3\}$, $\{\beta = 3 \text{ vs. } \beta = 4\}$, and {SSE vs. SZSE} when $\theta = 1.5$.

Fig. 7 shows the results of MM-DCCA (Hurst surface) displayed using a slipping fitting window $\{ [10, 50], [20, 100], \dots, [120, 600] \}$ for simulation data $\{\beta = 2 \text{ vs. } \beta = 3\}$ and $\{\beta = 3 \text{ vs. } \beta = 4\}$, and real data {SSE vs. SZSE} with threshold

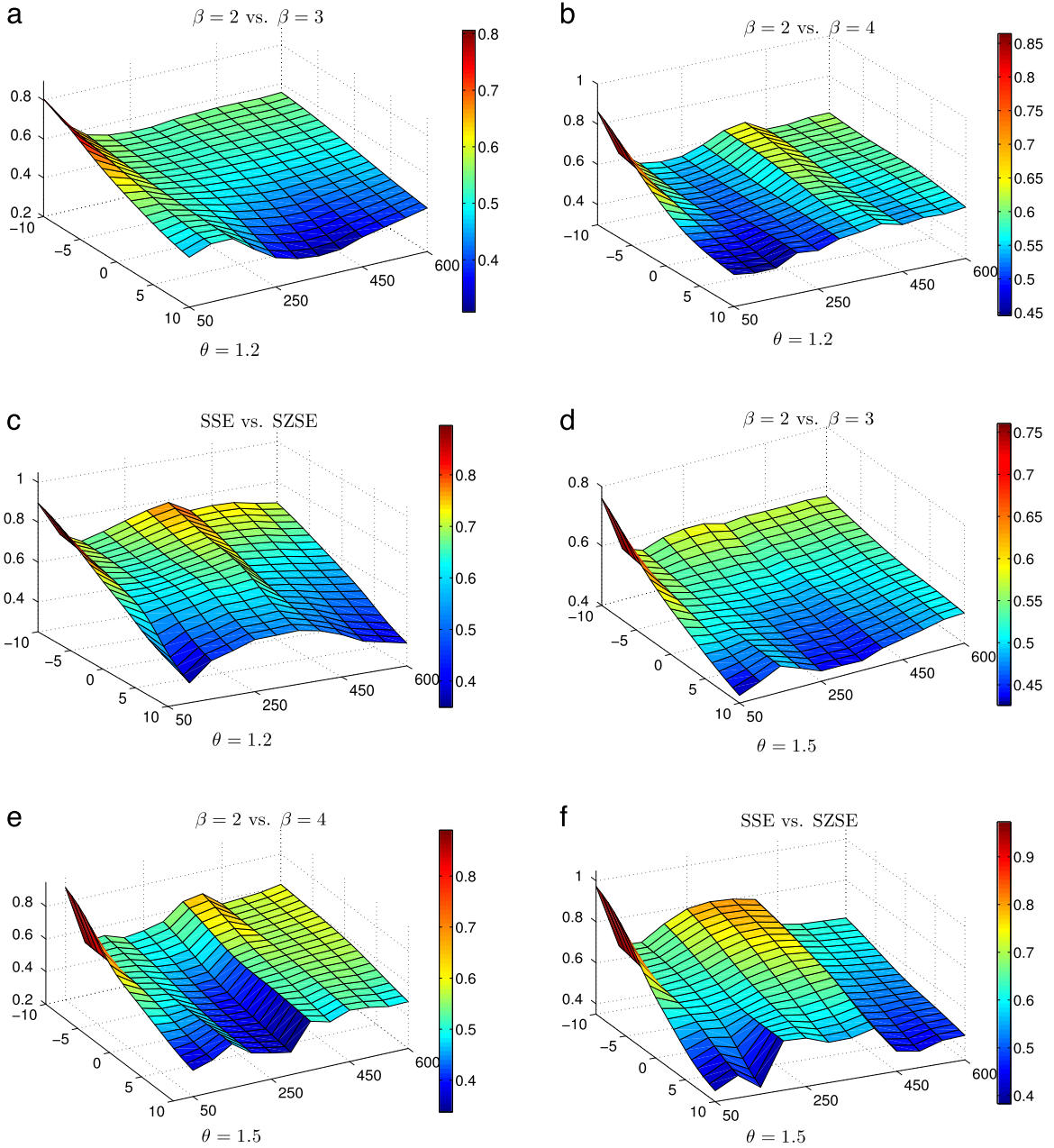


Fig. 7. (a)(b)(c) Hurst surfaces of return intervals from $\{\beta = 2$ vs. $\beta = 3\}$, $\{\beta = 3$ vs. $\beta = 4\}$ and $\{SSE$ vs. $SZSE\}$ when $\theta = 1.2$. (d)(e)(f) Hurst surfaces of return intervals from $\{\beta = 2$ vs. $\beta = 3\}$, $\{\beta = 3$ vs. $\beta = 4\}$ and $\{SSE$ vs. $SZSE\}$ when $\theta = 1.5$.

values $\theta = 1.2$ and $\theta = 1.5$ and a range of q from -10 to 10 . As mentioned above, when the power-law exponent $h_{xy}(q, s)$ is a constant, the market is monofractal, otherwise it is multifractal. Using this method, by observing the shape of Hurst surface we can distinguish the cross-correlation properties in all the available scales simultaneously. Fig. 7(a)–(c) show that the shapes of the three Hurst surfaces are similar, especially in Fig. 7(a) and (c), and that $\{\beta = 2$ vs. $\beta = 3\}$ and $\{SSE$ vs. $SZSE\}$ are multifractal in both small and large scales. In addition, $\{\beta = 2$ vs. $\beta = 4\}$ and $\{SSE$ vs. $SZSE\}$ show a similar oscillation on the Hurst surface. Fig. 7(d)–(f) show that when $\theta = 1.5$ these three plots are multifractal, and that $\{\beta = 2$ vs. $\beta = 4\}$ exhibits oscillations on the Hurst surface similar to those on the Hurst surface $\{SSE$ vs. $SZSE\}$.

Tables 2 and 3 provide the numerical results of the generalized Hurst exponent $h(q)$, where $q \in \{-10, -9, \dots, 9, 10\}$. Here we select the small scale $[10, 50]$, middle scale $[60, 300]$, and large scale $[120, 600]$ to illustrate the cross-correlations of the different return interval series. The two tables show that the value of cross-correlation exponent $h_{xy}(q)$ decreases when q increases. Thus different values of $h_{xy}(q)$ for different orders of q are clearly multifractal. As in all other Hurst exponent

Table 2
Generalized Hurst exponents $h_{xy}(q)$ of return intervals with $\theta = 1.2$.

q	$\beta = 2$ vs. $\beta = 3$			$\beta = 2$ vs. $\beta = 4$			SSE vs. SZSE		
	s_{ss}	s_{ms}	s_{ls}	s_{ss}	s_{ms}	s_{ls}	s_{ss}	s_{ms}	s_{ls}
$q = -10$	0.8058	0.5419	0.5546	0.8643	0.5883	0.6176	0.8957	0.7663	0.6938
$q = -9$	0.7902	0.5381	0.5508	0.8414	0.5848	0.6140	0.8824	0.7564	0.6826
$q = -8$	0.7720	0.5344	0.5465	0.8150	0.5810	0.6105	0.8668	0.7458	0.6701
$q = -7$	0.7514	0.5309	0.5417	0.7853	0.5772	0.6073	0.8489	0.7348	0.6563
$q = -6$	0.7287	0.5274	0.5368	0.7528	0.5733	0.6045	0.8286	0.7237	0.6416
$q = -5$	0.7048	0.5392	0.5302	0.7191	0.5695	0.6023	0.8065	0.7130	0.6262
$q = -4$	0.6806	0.5241	0.5269	0.6860	0.5657	0.6007	0.7834	0.7032	0.6106
$q = -3$	0.6571	0.5186	0.5209	0.6553	0.5620	0.5998	0.7602	0.6949	0.5949
$q = -2$	0.6351	0.5208	0.5194	0.6270	0.5586	0.5995	0.7371	0.6877	0.5793
$q = -1$	0.6148	0.5175	0.5086	0.6008	0.5554	0.5994	0.7138	0.6811	0.5637
$q = 0$	0.5958	0.5139	0.5012	0.5765	0.5527	0.5988	0.6893	0.6722	0.5470
$q = 1$	0.5784	0.5099	0.4935	0.5543	0.5501	0.5982	0.6682	0.6640	0.5316
$q = 2$	0.5616	0.5049	0.4858	0.5346	0.5480	0.5962	0.6469	0.6507	0.5142
$q = 3$	0.5452	0.5001	0.4779	0.5178	0.5460	0.5932	0.6258	0.6337	0.4953
$q = 4$	0.5293	0.4941	0.4703	0.5040	0.5441	0.5890	0.6033	0.6189	0.4747
$q = 5$	0.5141	0.4772	0.4628	0.4931	0.5422	0.5840	0.5789	0.5929	0.4529
$q = 6$	0.4999	0.4608	0.4557	0.4843	0.5398	0.5784	0.5545	0.5729	0.4312
$q = 7$	0.4870	0.4506	0.4489	0.4771	0.5372	0.5725	0.5323	0.5548	0.4110
$q = 8$	0.4755	0.4402	0.4424	0.4709	0.5343	0.5666	0.5130	0.5391	0.3931
$q = 9$	0.4655	0.4306	0.4364	0.4652	0.5314	0.5608	0.4967	0.5257	0.3778
$q = 10$	0.4570	0.4203	0.4307	0.4598	0.5284	0.5553	0.4831	0.5145	0.3648

Note: s_{ss} , s_{ms} and s_{ls} stand for small scale [10, 50], middle scale [60, 300] and large scale [120, 600], respectively.

Table 3
Generalized Hurst exponents $h_{xy}(q)$ of return intervals with $\theta = 1.5$.

q	$\beta = 2$ vs. $\beta = 3$			$\beta = 2$ vs. $\beta = 4$			SSE vs. SZSE		
	s_{ss}	s_{ms}	s_{ls}	s_{ss}	s_{ms}	s_{ls}	s_{ss}	s_{ms}	s_{ls}
$q = -10$	0.7606	0.5838	0.5658	0.8901	0.5659	0.6139	0.9733	0.8055	0.6154
$q = -9$	0.7416	0.5731	0.5611	0.8681	0.5548	0.6109	0.9572	0.7989	0.6081
$q = -8$	0.7201	0.5619	0.5562	0.8405	0.5422	0.6083	0.9373	0.7914	0.6001
$q = -7$	0.6964	0.5504	0.5512	0.8059	0.5381	0.6079	0.9129	0.7828	0.5912
$q = -6$	0.6715	0.5392	0.5462	0.7638	0.5259	0.6048	0.8832	0.7731	0.5819
$q = -5$	0.6468	0.5285	0.5412	0.7155	0.5226	0.6018	0.8479	0.7619	0.5720
$q = -4$	0.6238	0.5186	0.5364	0.6662	0.5159	0.5989	0.8076	0.7494	0.5620
$q = -3$	0.6032	0.5098	0.5319	0.6232	0.5102	0.5960	0.7644	0.7357	0.5521
$q = -2$	0.5849	0.5018	0.5278	0.5902	0.5079	0.5929	0.7211	0.7210	0.5426
$q = -1$	0.5684	0.4947	0.5241	0.5650	0.5048	0.5893	0.6807	0.7057	0.5340
$q = 0$	0.5528	0.4884	0.5212	0.5439	0.5009	0.5849	0.6445	0.6896	0.5266
$q = 1$	0.5383	0.4824	0.5184	0.5245	0.4789	0.5787	0.6126	0.6747	0.5197
$q = 2$	0.5241	0.4767	0.5164	0.5139	0.4659	0.5727	0.5826	0.6592	0.5142
$q = 3$	0.5101	0.4713	0.5147	0.5048	0.4496	0.5647	0.5528	0.6437	0.5093
$q = 4$	0.4963	0.4641	0.5132	0.4846	0.4359	0.5556	0.5228	0.6280	0.5047
$q = 5$	0.4828	0.4659	0.5117	0.4639	0.4142	0.5453	0.4940	0.6123	0.4998
$q = 6$	0.4698	0.4608	0.5102	0.4433	0.3959	0.5347	0.4682	0.5970	0.4944
$q = 7$	0.4575	0.4556	0.5084	0.4234	0.3700	0.5240	0.4465	0.5825	0.4883
$q = 8$	0.4459	0.4498	0.5065	0.4049	0.3659	0.5137	0.4289	0.5692	0.4820
$q = 9$	0.4353	0.4446	0.5044	0.3882	0.3562	0.5040	0.4147	0.5573	0.4757
$q = 10$	0.4256	0.4395	0.5027	0.3735	0.3459	0.4902	0.4032	0.5467	0.4697

Note: s_{ss} , s_{ms} and s_{ls} stand for small scale [10, 50], middle scale [60, 300] and large scale [120, 600], respectively.

calculations, we interpret the values of $h_{xy}(q)$ as follows [12,24]. When $h < 0.5$ the cross-correlations between the two time series are antipersistent. When $h = 0.5$ there are no cross-correlations or only short-term cross-correlations between the two time series. When $h > 0.5$ the cross-correlations between the two time series are long-term. The higher the h , the stronger the cross-correlations. The scaling exponent $h(2)$ is the well-known Hurst exponent, and Table 2 shows that all the $h(2)$ values at different scales for $\{\beta = 2$ vs. $\beta = 4\}$ and $\{SSE$ vs. $SZSE\}$ are bigger than 0.5, which means that the cross-correlations of return intervals from the simulation data and the real data are strongly persistent. When we examine the Hurst surface we see that the scaling multifractal and cross-correlation properties of the return interval series of the simulation data are similar to those of real market indices.

The relationships between classical multifractal scaling exponents $\tau_{xy}(q) = qh_{xy}(q) - 1$ are similar [11]. When $\tau_{xy}(q)$ is linear with q , the cross-correlation of the correlated series is monofractal, otherwise it is multifractal. Fig. 8 shows plots of the multiple behaviors of multifractal exponents $\tau_{xy}(q)$ of return intervals for the simulation data $\{\beta = 2$ vs. $\beta = 3\}$, $\{\beta = 3$ vs. $\beta = 4\}$, and real stock data $\{SSE$ vs. $SZSE\}$ when $\theta = 1.2$. Here the subplot is the corresponding Hurst surface in each

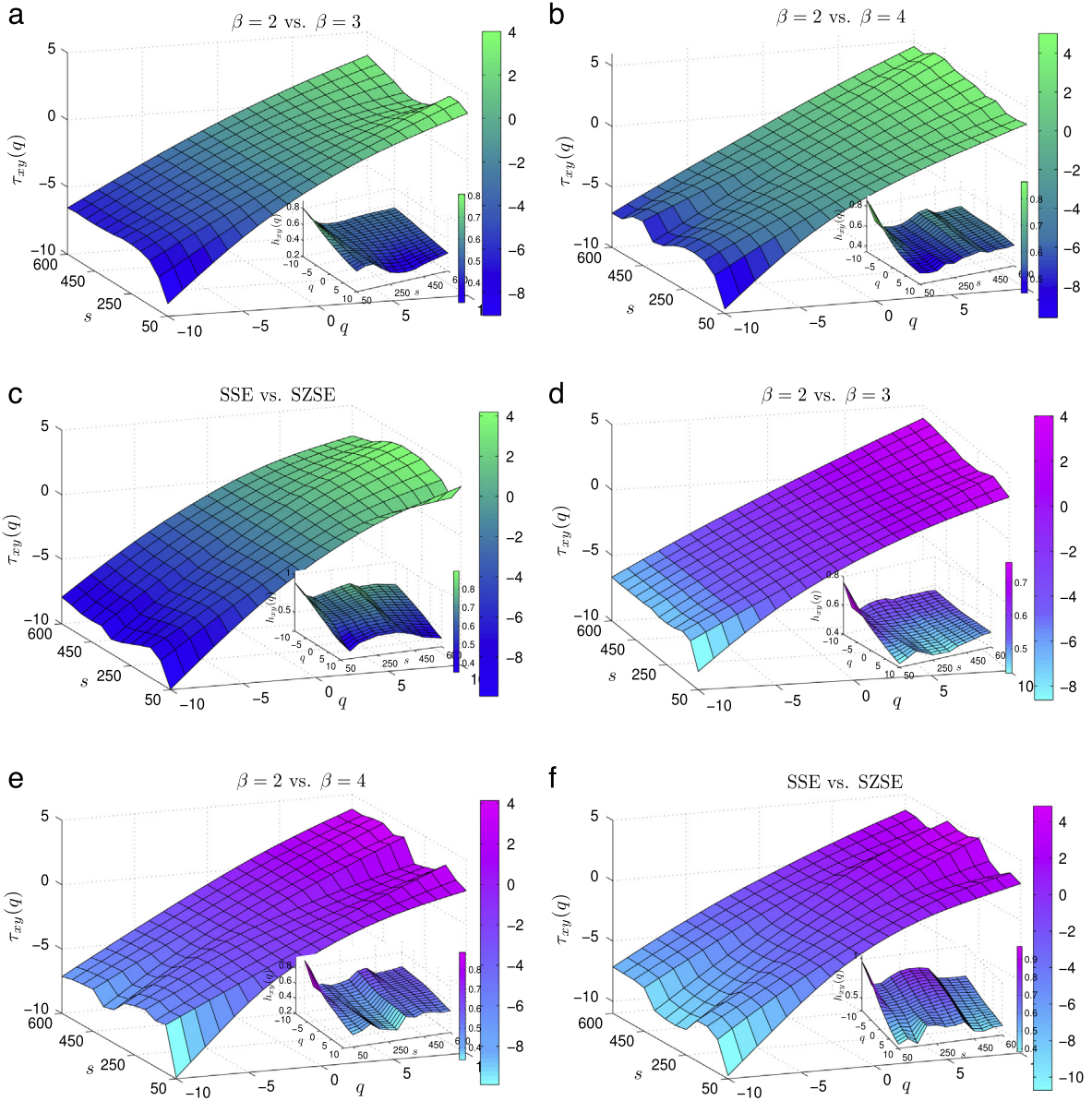


Fig. 8. (a)(b)(c) The exponents $\tau_{xy}(q)$ of return intervals from the simulation data $\{\beta = 2 \text{ vs. } \beta = 3\}$, $\{\beta = 3 \text{ vs. } \beta = 4\}$ and the real data {SSE vs. SZSE} when $\theta = 1.2$. (d)(e)(f) The exponents $\tau_{xy}(q)$ of return intervals from the simulation data $\{\beta = 2 \text{ vs. } \beta = 3\}$, $\{\beta = 3 \text{ vs. } \beta = 4\}$ and the real data {SSE vs. SZSE} when $\theta = 1.5$.

plot. These plots show that $\tau_{xy}(q)$ is nonlinearly dependent on q and is empirical evidence that multifractality exists in the six pairs of return intervals.

Using the Legendre transformation we obtain $\alpha = h_{xy}(q) + qh'_{xy}(q)$, and $f(\alpha) = q[\alpha - h_{xy}(q)] + 1$, where $h'_{xy}(q)$ denotes the derivative of $h_{xy}(q)$ with respect to q , and α is the Hölder exponent or singularity strength that characterizes the singularities in the time series. For multifractality, different portions are characterized by different α values and produce a spectrum $f(\alpha)$. We estimate multifractality strength using the width of the multifractal spectrum, which is given by $\Delta\alpha = \alpha_{\max} - \alpha_{\min}$. Fig. 9 shows the multiscale multifractal spectrum $f(\alpha)$ of the return intervals for $\theta = 1.2$ and $\theta = 1.5$. At the y-axis, 1, 2, 3 is multifractal spectrum $f(\alpha)$ of $\{\beta = 2 \text{ vs. } \beta = 3\}$, $\{\beta = 3 \text{ vs. } \beta = 4\}$, and {SSE vs. SZSE} when $\theta = 1.2$. Here 4, 5, 6 is the multifractal spectrum $f(\alpha)$ of $\{\beta = 2 \text{ vs. } \beta = 3\}$, $\{\beta = 3 \text{ vs. } \beta = 4\}$, and {SSE vs. SZSE} when $\theta = 1.5$. Each pair of return intervals have 12 multifractal spectrum $f(\alpha)$ curves under the moving window $\{[10, 50], [20, 100], \dots, [120, 600]\}$.

Tables 4 and 5 show the range of multifractal degrees Δh , $\Delta\alpha$, and Δf for the simulation return intervals and the real series, where $\Delta h = h(q_{\min}) - h(q_{\max})$, $\Delta f = f(\alpha_{\min}) - f(\alpha_{\max})$. Note that in all these time series the values of Δh for the return intervals are far from zero. This suggests that both simulation data and real data have multifractality properties

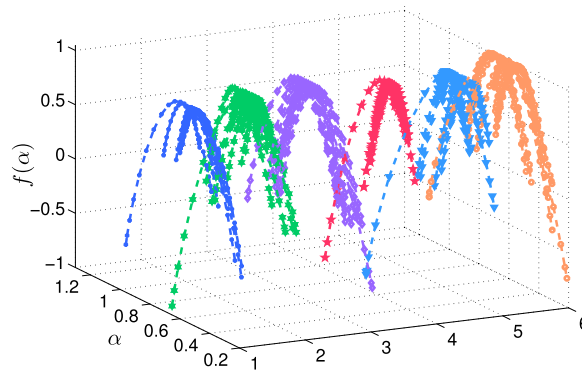


Fig. 9. Multifractal spectra $f(\alpha)$ of return intervals for $\theta = 1.2$ and $\theta = 1.5$ from $\{\beta = 2$ vs. $\beta = 3\}$, $\{\beta = 3$ vs. $\beta = 4\}$ and $\{\text{SSE vs. SZSE}\}$ in different scales.

Table 4

Multifractal strength and fractal asymmetric statistics of return intervals when $\theta = 1.2$.

Scale	$\beta = 2$ vs. $\beta = 3$			$\beta = 2$ vs. $\beta = 4$			SSE vs. SZSE		
	Δh	$\Delta\alpha$	Δf	Δh	$\Delta\alpha$	Δf	Δh	$\Delta\alpha$	Δf
[10, 50]	0.3488	0.4832	0.1723	0.4044	0.4674	0.3897	0.4125	0.5936	0.0499
[20, 100]	0.1524	0.2419	0.2345	0.1902	0.3259	0.3503	0.3726	0.4894	-0.3013
[30, 150]	0.0687	0.1324	0.4692	0.1145	0.2266	0.1794	0.2255	0.3338	-0.7981
[40, 200]	0.1216	0.2374	-0.4132	0.0553	0.1163	0.3498	0.2233	0.3840	-0.3709
[50, 250]	0.1823	0.2769	-0.5889	0.0612	0.1254	-0.0971	0.2213	0.3983	-0.0690
[60, 300]	0.2119	0.3092	-0.7396	0.0599	0.1195	0.1108	0.2517	0.4398	0.0763
[70, 350]	0.2367	0.3425	-0.5575	0.0982	0.1533	-0.2681	0.2686	0.4519	-0.0982
[80, 400]	0.2329	0.3601	-0.5234	0.0975	0.1563	0.0830	0.2288	0.3776	0.0826
[90, 450]	0.1996	0.3221	-0.3046	0.0674	0.0916	-0.0252	0.2733	0.4532	0.0535
[100, 500]	0.1757	0.2855	-0.1620	0.0549	0.0750	-0.0636	0.3213	0.4969	-0.0285
[110, 550]	0.1487	0.2399	-0.1392	0.0731	0.1693	0.0228	0.3229	0.5025	-0.0444
[120, 600]	0.1292	0.2096	-0.0442	0.0622	0.1421	-0.0862	0.3290	0.5100	-0.1021

Table 5

Multifractal strength and fractal asymmetric statistics of return intervals when $\theta = 1.5$.

Scale	$\beta = 2$ vs. $\beta = 3$			$\beta = 2$ vs. $\beta = 4$			SSE vs. SZSE		
	Δh	$\Delta\alpha$	Δf	Δh	$\Delta\alpha$	Δf	Δh	$\Delta\alpha$	Δf
[10, 50]	0.3350	0.4713	0.1029	0.5294	0.5677	-0.2561	0.5701	0.6694	-0.2390
[20, 100]	0.1203	0.1970	0.0019	0.1289	0.1976	-0.3217	0.2791	0.4253	0.1728
[30, 150]	0.0608	0.1012	-0.2683	0.0716	0.1479	0.5625	0.2804	0.3199	-0.4655
[40, 200]	0.1110	0.2138	0.5769	0.1143	0.1746	0.2949	0.2237	0.3323	-0.5735
[50, 250]	0.1491	0.2781	-0.5162	0.1579	0.2786	-0.6611	0.2032	0.3370	0.3943
[60, 300]	0.1942	0.2187	-0.5521	0.2081	0.3435	0.4386	0.2589	0.4096	-0.1969
[70, 350]	0.1331	0.2519	0.4273	0.1413	0.2747	0.6480	0.2506	0.3929	-0.3508
[80, 400]	0.1149	0.2186	-0.4506	0.1929	0.3489	0.3872	0.2021	0.3501	-0.3784
[90, 450]	0.1012	0.1989	0.5324	0.0584	0.1202	-0.0436	0.1916	0.3088	-0.1476
[100, 500]	0.0866	0.1747	-0.4476	0.0756	0.1469	-0.2114	0.1933	0.3190	-0.1910
[110, 550]	0.0725	0.1435	-0.3585	0.1074	0.1895	-0.4349	0.1559	0.2742	0.1287
[120, 600]	0.0637	0.1291	0.2896	0.1266	0.2197	-0.3459	0.1458	0.2672	0.2459

across a range of scales. Tables 4 and 5 also show the calculation results of $\Delta\alpha$, and we see that the values of $\Delta\alpha$ exhibit the same trend as those of Δh . Note that in Tables 4 and 5 the spectrum is wider in small scales than in large scales because the multifractal properties are richer in small scales. The Δf value is the asymmetry of the multifractal spectra. From the calculation results in Tables 4 and 5, $\Delta f > 0$ in the small scale [10, 50] for all the simulation and real data, but in [120, 600] $\Delta f < 0$ indicate that the asymmetry of the return intervals of the model is similar to that in the multifractal spectra of the real return intervals.

6. Conclusion

Using a Potts dynamic system we have developed a financial model to investigate the volatility behaviors of return interval time series. By applying the LZC method and using different exponents, we find that the trend of the LZC complexity of simulation data is the same as in real data, and when $\theta = 1.5, 1.8, 2$ the trend of the LZC results of all the return intervals is the same. We also find that increasing q decreases the randomness of the return intervals. In the empirical analysis of the

MM-DCCA, we examine the shape of the Hurst surface and find that the return intervals in the proposed model data have similar multifractal cross-correlation results as real stock data. The numerical values of $h(2) > 0.5$ and $\Delta h > 0.05$ in both simulation data and real data verifies the multifractality and cross-correlation properties in all the experimental scales. The behavior of the return intervals in the empirical results are statistically similar to those in the simulated data and the real market data and confirm the rationality in the construction of this proposed price model.

Acknowledgments

The authors were supported by National Natural Science Foundation of China Grant No. 71271026 and by the Fundamental Research Funds for the Central Universities No. S16JB00100.

References

- [1] H.E. Stanley, V. Plerou, Scaling and universality in economics: empirical results and theoretical interpretation, *Quant. Finance* 1 (2001) 563–567.
- [2] L.A.N. Amaral, S.V. Buldyrev, S. Havlin, M.A. Salinger, H.E. Stanley, Power law scaling for a system of interacting units with complex internal structure, *Phys. Rev. Lett.* 80 (1998) 1385–1388.
- [3] J.P. Bouchaud, M. Potters, *Theory of Financial Risk and Derivative Pricing: From Statistical Physics to Risk Management*, Cambridge University Press, Cambridge, 2003.
- [4] H.E. Stanley, X. Gabaix, P. Gopikrishnan, V. Plerou, Economic fluctuations and statistical physics: the puzzle of large fluctuations, *Nonlinear Dynam.* 44 (2006) 329–340.
- [5] J.D. Farmer, S. Joshi, The price dynamics of common trading strategies, *J. Econ. Behav. Organ.* 49 (2002) 149–171.
- [6] E.E. Peters, *Fractal Market Analysis: Applying Chaos Theory to Investment and Economics*, Wiley, New York, 1994.
- [7] R.S. Tsay, *Analysis of Financial Time Series*, John Wiley & Sons, Hoboken, USA, 2005.
- [8] D. Grech, G. Pamula, Multifractality of nonlinear transformations with application in finances, *Acta Phys. Polon. A* 123 (2013) 529–537.
- [9] W.J. Hong, J. Wang, Multiscale behavior of financial time series model I from Potts dynamic system, *Nonlinear Dynam.* 78 (2014) 1065–1077.
- [10] X. Gabaix, P. Gopikrishnan, V. Plerou, H.E. Stanley, A theory of power-law distributions in financial market fluctuations, *Nature* 423 (2003) 267–270.
- [11] H.L. Niu, J. Wang, Volatility clustering and long memory of financial time series and financial price model, *Digit. Signal Process.* 23 (2013) 489–498.
- [12] T. Lux, Estimation of an agent-based model of investor sentiment formation in financial markets, *J. Econom. Dynam. Control* 36 (2012) 1284–1302.
- [13] J.H. Zhang, P. McBurney, K. Musial, Convergence of trading strategies in continuous double auction markets with boundedly-rational networked traders, *Rev. Quant. Finance Account.* (2017). <http://dx.doi.org/10.1007/s11156-017-0631-3>.
- [14] F. Black, M. Scholes, The pricing of options and corporate liabilities, *J. Polit. Econ.* 81 (1973) 637–654.
- [15] G.F. Gu, W.X. Zhou, Emergence of long memory in stock volatility from a modified Mike–Farmer model, *EPL–Europhys. Lett.* 86 (2000) 48002.
- [16] R. Durrett, *Lecture Notes on Particle Systems and Percolation*, Wadsworth & Brooks, Pacific Grove–California, 1998.
- [17] T. Lux, M. Marchesi, Scaling and criticality in a stochastic multiagent model of a financial market, *Nature* 397 (1999) 498–500.
- [18] E. Zivot, J.H. Wang, *Modeling Financial Time Series with S-PLUS*, Springer, New York, 2006.
- [19] S. Mike, J.D. Farmer, An empirical behavioral model of liquidity and volatility, *J. Econom. Dynam. Control* 32 (2008) 200–234.
- [20] D. Stauffer, T.J.P. Penna, Crossover in the Cont–Bouchaud percolation model for market fluctuations, *Physica A* 256 (1998) 284–290.
- [21] Y. Yu, J. Wang, Lattice-oriented percolation system applied to volatility behavior of stock market, *J. Appl. Stat.* 39 (2012) 785–797.
- [22] J.H. Zhang, J. Wang, Modeling and simulation of the market fluctuations by the finite range contact systems, *Simul. Model. Pract. Theory* 18 (2010) 910–925.
- [23] S. Bornholdt, F. Wagner, Stability of money: phase transitions in an Ising economy, *Physica A* 316 (2002) 453–468.
- [24] S. Grollau, M.L. Rosinberg, G. Tarjus, The ferromagnetic q -state Potts model on three-dimensional lattices: a study for real values of q , *Physica A* 296 (2001) 460–482.
- [25] A. Krawiecki, Microscopic spin model for the stock market with attractor bubbling and heterogeneous agents, *Internat. J. Modern Phys. C* 16 (2005) 549–559.
- [26] W. Fang, J. Wang, Fluctuation behaviors of financial time series by a stochastic Ising system on a Sierpinski carpet lattice, *Physica A* 392 (2013) 4055–4063.
- [27] F. Wang, K. Yamasaki, S. Havlin, H.E. Stanley, Scaling and memory of intraday volatility return intervals in stock markets, *Phys. Rev. E* 73 (2006) 026117.
- [28] H. Hong, M. Liang, Fault severity assessment for rolling element bearings using the Lempel–Ziv complexity and continuous wavelet transform, *J. Sound Vib.* 320 (2009) 452–468.
- [29] J. Szczepański, J.M. Amigó, E. Wajnryb, M.V. Sanchez-Vives, Characterizing spike trains with Lempel–Ziv complexity, *Neurocomputing* 58–60 (2004) 79–84.
- [30] A. Fernández, M.I. López-Ibor, A. Turrero, et al., LempelZiv complexity in schizophrenia: a MEG study, *Clin. Neurophysiol.* 122 (2011) 2227–2235.
- [31] Y.H. Liu, P. Gopikrishnan, P. Cizeau, M. Meyer, C.K. Peng, H.E. Stanley, Statistical properties of the volatility of price fluctuations, *Phys. Rev. E* 62 (2000) 4493–4496.
- [32] P. Gopikrishnan, V. Plerou, Y.H. Liu, L.A.N. Amaral, X. Gabaix, H.E. Stanley, Scaling and correlation in financial time series, *Physica A* 287 (2000) 362–373.
- [33] B. Podobnik, H.E. Stanley, Detrended cross-correlation analysis: a new method for analyzing two nonstationary time series, *Phys. Rev. Lett.* 100 (2008) 084102.
- [34] J.W. Kantelhardt, S.A. Zschiegner, E. Koscielny-Bunde, S. Havlin, A. Bunde, H.E. Stanley, Multifractal detrended fluctuation analysis of nonstationary time series, *Physica A* 316 (2002) 87–114.
- [35] G.J. Wang, C. Xie, M. Lin, H.E. Stanley, Stock market contagion during the global financial crisis: A multiscale approach, *Finance Res. Lett.* 22 (2017) 163–168.
- [36] W.X. Zhou, Multifractal detrending cross-correlation analysis for two nonstationary signals, *Phys. Rev. E* 77 (2008) 066211.
- [37] G.F. Zebende, DCCA cross-correlation coefficient: quantifying level of cross-correlation, *Physica A* 390 (2011) 614–618.
- [38] M.F. da Silva, É.J.D.A.L. Pereira, A.M. da Silva Filho, A.P.N. de Castro, J.G.V. Miranda, G.F. Zebende, Quantifying cross-correlation between Ibovespa and Brazilian blue-chips: The DCCA approach, *Physica A* 424 (2015) 124–129.
- [39] F. Gliozzi, Simulation of potts models with real q and no critical slowing down, *Phys. Rev. E* 66 (2002) 016115.
- [40] R.J. Baxter, Potts model at the critical temperature, *J. Phys. C: Solid State Phys.* 6 (1973) 445.
- [41] Y. Deng, H.W.J. Blöte, B. Nienhuis, Backbone exponents of the two-dimensional q -state Potts model: a Monte Carlo investigation, *Phys. Rev. E* 69 (2004) 026114.
- [42] D. Lamberton, B. Lapeyre, *Introduction to Stochastic Calculus Applied To Finance*, Chapman and Hall/CRC, London, 2000.

- [43] S.M. Ross, *An Introduction to Mathematical Finance*, Cambridge University Press, Cambridge, 1999.
- [44] M.S. Santhanam, H. Kantz, Return interval distribution of extreme events and long-term memory, *Phys. Rev. E* 78 (2008) 051113.
- [45] F.Z. Wang, K. Yamasaki, S. Havlin, H.E. Stanley, Scaling and memory of intraday volatility return intervals in stock markets, *Phys. Rev. E* 73 (2006) 026117.
- [46] A. Lempel, J. Ziv, On the complexity of finite sequences, *IEEE Trans. Inform. Theory* 22 (1976) 75–81.
- [47] X.S. Zhang, R.J. Roy, E.W. Jensen, EEG complexity as a measure of depth of anesthesia for patients, *IEEE Trans. Biomed. Eng.* 48 (2001) 1424–1433.
- [48] B. Podobnik, D. Horvatic, A.M. Petersen, H.E. Stanley, Crosscorrelations between volume change and price change, *Proc. Natl. Acad. Sci. USA* 106 (2009) 22079–22084.
- [49] B. Podobnik, Z.Q. Jiang, W.X. Zhou, H.E. Stanley, Statistical tests for power-law cross-correlated processes, *Phys. Rev. E* 84 (2011) 066118.
- [50] B. Podobnik, I. Grosse, D. Horvatic, S. Ilic, P. Ch. Ivanov, H.E. Stanley, Quantifying cross-correlations using local and global detrending approaches, *Eur. Phys. J. B* 71 (2009) 243–250.
- [51] J. Gieraltowski, J.J. Zebrowski, R. Baranowski, Multiscale multifractal analysis of heart rate variability recordings with a large number of occurrences of arrhythmia, *Phys. Rev. E* 85 (2012) 021915.
- [52] Y. Wang, Y. Wei, C. Wu, Cross-correlations between Chinese A-share and B-share markets, *Physica A* 389 (2010) 5468–5478.
- [53] B. Podobnik, D.F. Fu, H.E. Stanley, P.C. Ivanov, Power-law auto-correlated stochastic processes with long-range cross-correlations, *Eur. Phys. J. B* 56 (2007) 47–52.
- [54] C.K. Peng, S. Havlin, H.E. Stanley, A.L. Goldberger, Quantification of scaling exponents and crossover phenomena in nonstationary heartbeat time series, *Chaos* 5 (1995) 82–87.